Metal-Organic Frameworks

Computational Identification and Experimental Demonstration of High-Performance Methane Sorbents

Karabi Nath[+], Alauddin Ahmed[+], Donald J. Siegel,* and Adam J. Matzger*

Abstract: Remarkable methane uptake is demonstrated experimentally in three metal-organic frameworks (MOFs) identified by computational screening: UTSA-76, UMCM-152 and DUT-23-Cu. These MOFs outperform the benchmark sorbent, HKUST-1, both volumetrically and gravimetrically, under a pressure swing of 80 to 5 bar at 298 K. Although high uptake at elevated pressure is critical for achieving this performance, a low density of high-affinity sites (coordinatively unsaturated metal centers) also contributes to a more complete release of stored gas at low pressure. The identification of these MOFs facilitates the efficient storage of natural gas via adsorption and provides further evidence of the utility of computational screening in identifying overlooked sorbents.

Natural gas (NG) is often cited as an important stepping-stone in the transition to low-carbon transportation fuels.[1,2] NG, comprising methane as the primary component, is an attractive gasoline alternative on account of its wide availability, established distribution network, high hydrogen to carbon ratio, and moderate carbon emissions. However, the low density of NG presents challenges for its storage that limit energy density and impede broad deployment in mobile applications such as vehicles. Particularly, the volumetric energy density of NG, which impacts the driving range of a vehicle, is much lower than that of gasoline: uncompressed NG has an energy density of 0.04 MJ L^{-1} while gasoline exhibits a value of 32.4 MJ L^{-1}.[3] Physical approaches to improve volumetric storage density include

liquefaction at low temperatures ($\sim$110 K, liquefied natural gas, LNG with an energy density of $\sim$22.2 MJ L^{-1}) or compression at high pressures ($\sim$250 bar, CNG, compressed natural gas with an energy density of $\sim$9 MJ L^{-1}).[4] CNG requires the use of bulky and expensive fuel tanks, and multistage compressors.[5] LNG allows for lower pressures but with the drawback of complex tank designs and pressure buildup upon extended storage.[6] Adsorbed natural gas (ANG) is a promising alternative to compression and liquefaction.[7] Adsorbents can potentially store NG at high densities at modest pressures ($\sim$35–80 bar), which translates to less costly tank designs.

MOFs with high porosity, high surface area, and tunability in structure have emerged as promising materials for ANG.[8–13] The most common proxy for ANG performance is methane storage capacity. For vehicular applications, a suitable adsorbent should exhibit a combination of high methane uptake at the maximum (filled state) storage pressure (65 or 80 bar)[14,15] with low uptake at the minimum desorption pressure (5 bar), resulting in a high *usable* capacity (residual gas stored at pressures below 5 bar is insufficient to power an internal combustion engine).[9,13] The *usable* (or *deliverable*) uptake should be distinguished from *total* uptake. The former is a practical metric of performance, whereas the latter represents the maximum gas stored at high pressure and does not account for any residual gas present at low pressures.

Among the many possible MOFs, HKUST-1 is commonly cited as a benchmark methane adsorbent, given its high *total* methane capacity [267 cm^3 (STP) cm^{-3} at 65 bar and 272 cm^3 (STP) cm^{-3} at 80 bar] and excellent *deliverable* capacity [190 cm^3 (STP) cm^{-3} (65–5 bar) and 200 cm^3 (STP) cm^{-3} (80–5 bar)].[13,16] Tens of thousands of MOFs have been synthesized, yet only a fraction have been examined experimentally as methane sorbents due to the time-consuming nature of these measurements. Therefore, computational screening has emerged as a useful tool for finding optimal MOFs for ANG.[17–26] Here, high-throughput Grand Canonical Monte Carlo (GCMC) simulations are used to

[*] Dr. K. Nath,[+] Prof. Dr. A. J. Matzger
Department of Chemistry and Macromolecular Science and Engineering Program, University of Michigan
930 North University Avenue, Ann Arbor, MI 48109 (USA)
E-mail: matzger@umich.edu

Dr. A. Ahmed,[+] Prof. Dr. D. J. Siegel
Mechanical Engineering Department, University of Michigan
Ann Arbor, MI 48109 (USA)
and
Materials Science and Engineering, Applied Physics Program, and University of Michigan Energy Institute, University of Michigan
Ann Arbor, MI 48109 (USA)

Prof. Dr. D. J. Siegel
Current address: Walker Department of Mechanical Engineering, Texas Materials Institute and Oden Institute for Computational Engineering and Sciences, University of Texas at Austin
204 E. Dean Keeton Street, ETC II 5.160, Austin, TX 78712-1591 (USA)
E-mail: Donald.Siegel@austin.utexas.edu

[+] These authors contributed equally to this work.

identify promising MOFs whose capacities for methane uptake exceeds that of state-of-the-art materials. Experimental synthesis and methane uptake measurements reveal that three of these MOFs—UTSA-76, UMCM-152 and DUT-23-Cu—surpass the methane capacity of HKUST-1 as well as for other noteworthy methane sorbents (Table S6), providing a new high-water mark for methane storage materials.[27] An additional distinguishing feature of this work is the use of interatomic potentials that explicitly account for the presence of coordinatively unsaturated sites (CUS).[28–30] CUS MOFs used in our calculations were identified by the CoRE 2019 database based on a python code developed by Haldoupis (*GitHub—Emmhald/Open_metal_detector*, n.d.). Figure 1 shows the predicted *usable* CH_4 capacities for 11185 MOFs from the CoRE[31] (2019) database at 298 K calculated using GCMC. The database includes MOFs with and without CUS. Initial screening was performed with the DREIDING(MOF)/TraPPE(CH_4)[32,33] potential for non-CUS MOFs and with a potential that accounts for CH_4-CUS interactions.[28] These data are shown in Figure 1. Subsequently, a portion of this data set was re-evaluated with an additional set of interatomic potentials: UFF(MOF)/TraPPE(CH_4)[32,34] for non-CUS MOFs and UFF(MOF)/9-site(CH_4)[29,30,34] for CUS MOFs.

In contrast to previous studies, two separate sets of interatomic potential parameters were used for CUS and non-CUS MOFs to identify high-capacity materials that were previously overlooked due to limitations of general interatomic potentials (Table S1). Notably, very few studies employ both computational and experimental approaches to demonstrate record-setting MOFs.[27] The potentials used here yielded superior agreement with the experimentally measured isotherms of the MOFs, as shown in Table 1. Two isothermal "pressure swing" operating conditions at 298 K are considered: a swing between 65 and 5 bar, and between 80 and 5 bar. From these calculations, 95 CUS MOFs are predicted to surpass both *usable* volumetric and gravimetric CH_4 capacities of HKUST-1[13,16] (190 cm^3 (STP) cm^{-3} and 0.154 $g\,g^{-1}$) for a pressure swing between 65 and 5 bar while 96 CUS MOFs outperform HKUST-1[13,16,35] (200 cm^3 (STP) cm^{-3} and 0.162 $g\,g^{-1}$) for a pressure swing of 80 to 5 bar (Tables S2 and S3). A total of only 8 non-CUS MOFs were predicted to surpass HKUST-1 (Tables S4 and S5). UMCM-152 and DUT-23-Cu were identified as sorbents with the potential to exceed the performance of HKUST-1.[36,37] These MOFs were chosen based on their predicted high performance and synthetic accessibility. In addition, UTSA-76 was evaluated as a second benchmark material because it has been reported to outperform HKUST-1 in the pressure range of 5–65 bar.[38] Computational predictions are based on idealized MOF models that typically assume that all solvent, un-reacted salt, and disorder have been removed
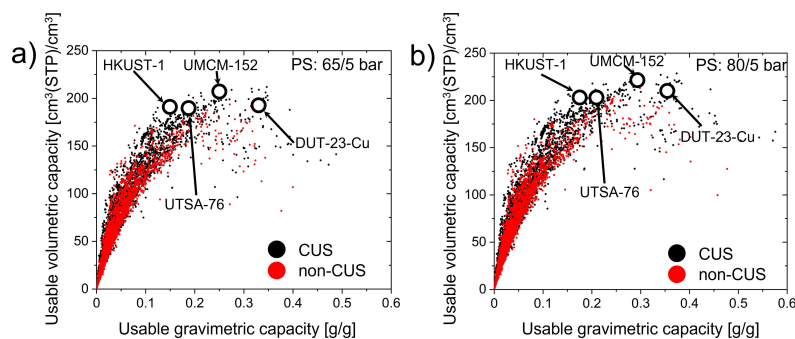

Figure 1. Usable volumetric capacity of CUS and non-CUS MOFs as a function of gravimetric capacity at 298 K under pressure swing between a) 5 and 65 bar and b) 5 and 80 bar.

Table 1: *Usable* CH_4 capacities and crystallographic properties of high-capacity MOFs.

MOFs	CUS density[b] [mmoles g^{-1}]	Gravimetric surface area [$m^2\,g^{-1}$] Expt./Calc.	Pore Volume [$cm^3\,g^{-1}$] Expt./Calc.	Pressure swing 65 to 5 bar at 298 K		Pressure swing 80 to 5 bar at 298 K	
				Gravimetric capacity [$g\,g^{-1}$] Expt./Calc.	Volumetric capacity [cm^3 (STP) cm^{-3}] Expt./Calc.	Gravimetric capacity [$g\,g^{-1}$] Expt./Calc.	Volumetric capacity [cm^3 (STP) cm^{-3}] Expt./Calc.
HKUST-1[a]	4.96	1850/2159	0.78/0.81	0.154/0.150	190/184	0.162/0.158	200/195
UTSA-76 (this work)	3.77	2700/3205	1.09/1.08	0.200/0.194	195/189	0.215/0.207	210/201
UMCM-152 (this work)	3.13	3430/3480	1.45/1.38	0.247/0.259	207/205	0.271/0.276	226/219
DUT-23-Cu (this work)	N/A	5300/4636	2.23/1.99	0.332/0.333	190/192	0.377/0.361	216/208

[a] *Usable* capacities of HKUST-1 under 65/5 and 80/5 bar pressure swing were collected from Ref. [13, 16] respectively. Measured crystallographic properties of HKUST-1 were collected from Ref. [16]. [b] CUS density of MOFs was calculated based on the crystallographic information files.

from the crystal structure. As these components can play a role in stabilizing some MOFs there is no guarantee that a given MOF can be realized experimentally in its fully activated form. In fact, a previous study[39] of hydrogen sorbents found that many promising MOFs identified from screening databases of experimentally-known MOFs were not possible to synthesize with surface areas close to the predicted values due to various modes of collapse[40,41] or inadequate activation.[42,43] Therefore, experimental validation of predicted hits is critical.

UTSA-76 (Figure 2a) is a CUS MOF, synthesized from a tetracarboxylate pyrimidine linker (5,5′-(pyrimidine-2,5-diyl) diisophthalic acid) that exhibits a BET surface area of 2700 $m^2 g^{-1}$ and pore volume of 1.09 $cm^3 g^{-1}$ (at $P/P_0 = 0.95$) (Table 1 and Figure S9). UTSA-76 demonstrates *total* volumetric (TV) uptake of 251 cm^3 (STP) cm^{-3} at a pressure of 65 bar (298 K, Table 1) in accord with previous observations.[38] Improved capacity is achieved at 80 bar (266 cm^3 (STP) cm^{-3}) signaling that saturation had not been achieved previously. These TV values are lower than HKUST-1 for both maximum pressures. However, UTSA-76 exhibits significantly improved *usable* volumetric (UV) capacity of 210 cm^3 (STP) cm^{-3} (80–5 bar) in comparison to HKUST-1 (200 cm^3 (STP) cm^{-3}). The undesirable higher uptake of HKUST-1 relative to UTSA-76 in the 0–5 bar region is ascribed to the presence of a higher density of CUS in HKUST-1, resulting in a larger density of methane molecules adsorbed at low pressures.[44] This observation is consistent with previous reports that the presence of CUS can have detrimental effects on the *usable* capacities of MOFs.[45,46]

UMCM-152 (Figure 2b) is assembled from Cu^{II} paddlewheel clusters connected through tetracarboxylated triphenyl benzene linkers (5′-(4-carboxyphenyl)-[1,1′:3′,1′′-terphenyl]-3,4′′,5-tricarboxylic acid) and has a smaller CUS density relative to UTSA-76 (Table 1). The linker has a trapezoidal geometry and two types of carboxylates:[36] one from the isophthalate group and the other is a para-benzoate unit. The structure is composed of two cages (pore diameters: ≈16.9 and 18.6 Å). One of the cages is formed from the faces of six linker molecules and twelve Cu^{II} paddlewheel clusters while the other cage is defined by the edges of twelve linkers and six Cu^{II} paddlewheels. These cages stack

in an alternate fashion. DUT-23-Cu (Figure 2c), on the other hand is a non-CUS MOF composed of dodecahedral mesoporous cages with pto-like topology, constructed from Cu^{II} and mixed linkers (4,4′-bypyridine and H_3BTB (1,3,5-tris(4-carboxyphenyl)benzene)).The dative ligands fully cap the copper paddlewheels blocking guest access to the metal sites.[37] The measured BET surface areas are 3430 $m^2 g^{-1}$ (UMCM-152) and 5300 $m^2 g^{-1}$ (DUT-23-Cu), with pore volumes (at $P/P_0 = 0.95$) of 1.45 $cm^3 g^{-1}$ and 2.23 $cm^3 g^{-1}$ respectively (Table 1 and Figure S10 and S11).

As predicted computationally, UMCM-152 exhibits remarkably high *usable* methane capacity that outperforms both HKUST-1 and UTSA-76, Table 1. The UV capacity of UMCM-152 is 207 cm^3 (STP) cm^{-3} (9% greater than HKUST-1 and 6% greater than UTSA-76) and 226 cm^3 (STP) cm^{-3} (13% > HKUST-1; 7% > UTSA-76) under 65–5 bar and 80–5 bar pressure swings, respectively, at 298 K. On the other hand, DUT-23-Cu exhibits a UV capacity of 190 cm^3 (STP) cm^{-3} (identical to HKUST-1 and below UTSA-76) and 216 cm^3 (STP) cm^{-3} (8% greater than HKUST-1 and 3% greater than UTSA-76) under a pressure swing of 65–5 bar and 80–5 bar, respectively, at 298 K. It should be noted that this performance is much higher than the Co analog: DUT-23-Co.[37]

Among all the MOFs examined, TV uptake is still the highest in the case of HKUST-1 in both the high- and low-pressure region. The increase in the UV capacities of UTSA-76, UMCM-152 and DUT-23-Cu relative to HKUST-1 is attributed to their comparatively low methane uptake at 5 bar (DUT-23-Cu: 21 cm^3 (STP) cm^{-3} < UMCM-152: 40 cm^3 (STP) cm^{-3} < UTSA-76: 56 cm^3 (STP) cm^{-3} < HKUST-1: 72 cm^3 (STP) cm^{-3}). From this trend it is apparent that the success of DUT-23-Cu is ascribed to less adsorbed CH_4 at low pressure due to a lack of electrostatic interactions between CH_4 molecules and CUS (CUS are absent in DUT-23-Cu), rather high uptake at high pressure. This is an important design concern, and its manifestation is more subtle than the phenomenon in low temperature hydrogen sorbents where the presence of CUS can degrade *deliverable* capacity dramatically.[28] Further, the uptake at 80 bar follows the order (DUT-23-Cu: 237 cm^3 (STP) cm^{-3} < UMCM-152: 266 cm^3 (STP) cm^{-3} ≈ UTSA-76: 266 cm^3 (STP) cm^{-3} < HKUST-1: 272 cm^3 (STP) cm^{-3}). Thus, larger pore

a) UTSA-76 b) UMCM-152 c) DUT-23-Cu
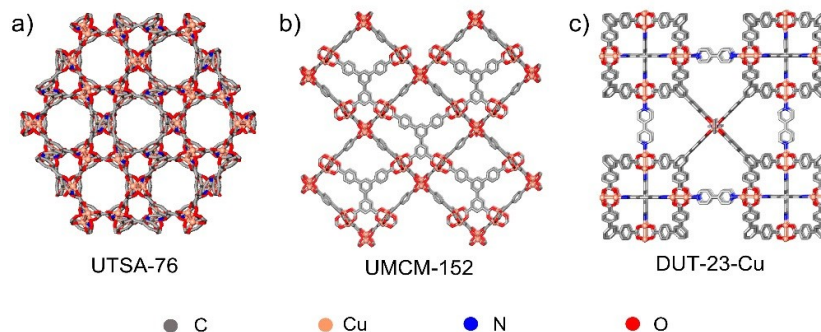
● C   ● Cu   ● N   ● O

Figure 2. Crystal structures of MOFs being assessed for methane uptake in the present study.

volume in DUT-23-Cu contributes to having relatively lower volumetric uptakes both at 5 bar (21 cm^3 (STP) cm^{-3}) and 80 bar (237 cm^3 (STP) cm^{-3}) respectively. The trend can be understood in the context of previous studies on IRMOF-8-RT, another MOF with large pores, where only 50–65 % of the pores are filled by adsorbed methane even at 89.4 bar.[47] Reduction of pore size with additional linker substituents resulted in higher volumetric uptake in the derivatives of IRMOF-8-RT.[48]

Although *deliverable* volumetric capacity is the primary figure of merit for an ANG system, gravimetric capacity also influences vehicular performance because it impacts the mass of the ANG system. Earlier studies have demonstrated that gravimetric capacity depends on the pore volume and BET surface area of MOFs.[9,49] For example, MOF-200,[50] MOF-210[50] and Al-soc-MOF-1[51] with high BET surface areas of 4530, 6240 and 5585 m^{2}g^{-1} respectively, have high gravimetric uptakes but all suffer from low volumetric uptakes. On the other hand, HKUST-1 possesses high volumetric methane uptake at the expense of poor gravimetric capacity. A strategy to design MOFs with high UV capacity without compromising gravimetric methane uptake requires balancing surface area and porosity.[52] In the present study, UTSA-76, UMCM-152 and DUT-23-Cu all outperform HKUST-1 in terms of their respective *total* gravimetric (TG) uptakes for pressures exceeding ≈ 30 bar. In fact, the TG uptake both at 65 and 80 bar follows the same order as the MOF's respective surface areas: HKUST-1: 1836 m^{2}g^{-1} < UTSA-76: 2700 m^{2}g^{-1} < UMCM-152: 3430 m^{2}g^{-1} < DUT-23-Cu: 5300 m^{2}g^{-1}. However, at 5 bar, the gravimetric uptake follows a similar trend as of volumetric capacity, Figure 3. The *usable* gravimetric (UG) capacities of all three MOFs exceeds HKUST-1 under both pressure swing conditions, Table 1.

In summary, the present study has identified promising MOFs for methane sorption computationally. Based on these predictions, three MOFs, UTSA-76, UMCM-152 and DUT-23-Cu, were synthesized and their measured capacities were observed to surpass the *usable* capacity of HKUST-1, the benchmark for methane storage, under pressure swing conditions (Figure 4). Specifically, UMCM-152 is demonstrated to outperform the volumetric deliverable capacities of all of the best MOFs, known so far, thus highlighting its promise in methane storage (Table S6). Although high uptake at elevated pressure is critical for achieving this performance, there is an additional requirement that the density of high affinity sites (coordinatively unsaturated metal centers) is low enough to allow relatively complete release of stored gas at low pressure. The utility of mining existing MOF databases for promising materials is demonstrated and provides an efficient discovery paradigm for measurements, such as high pressure methane storage, that are challenging experimentally.
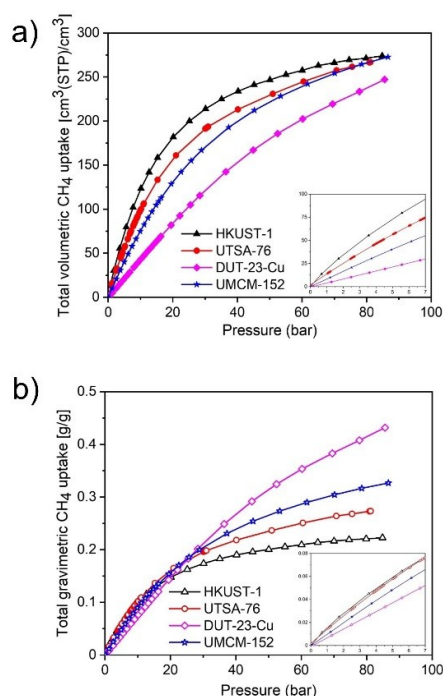

Figure 3. High pressure CH$_4$ isotherms. Measured *total* a) volumetric and b) gravimetric plots for UTSA-76, UMCM-152 and DUT-23-Cu. For comparison, the isotherm of HKUST-1[13,16] is also shown.
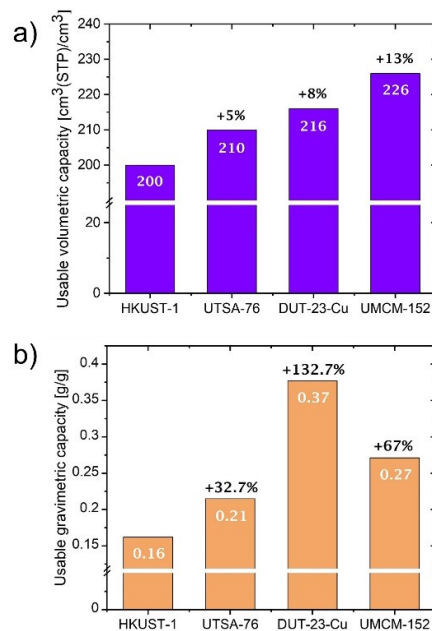

Figure 4. Comparison of measured *usable* capacities of top performing MOFs, HKUST-1,[13,16] UTSA-76, DUT-23-Cu and UMCM-152 on a a) volumetric and b) gravimetric basis. Capacities are reported under a pressure swing of 80–5 bar at 298 K.

Conflict of Interest

The authors declare no conflict of interest.

Data Availability Statement

The data that support the findings of this study are available on request from the corresponding author. The data are not publicly available due to privacy or ethical restrictions.

Keywords: Computational Screening · Deliverable Capacity · Interatomic Potentials · Metal Organic Framework (MOF) · Methane Storage

[1] A. Celzard, V. Fierro, *Energy Fuels* **2005**, *19*, 573–583.
[2] R. W. Howarth, R. Santoro, A. Ingraffea, *Clim. Change* **2011**, *106*, 679–690.
[3] Alternative Fuels Data Center, Fuel Properties Comparison, **2013**. http://www.afdc.energy.gov/fuels/fuel_comparison_chart.pdf.
[4] T. A. Makal, J.-R. Li, W. Lu, H.-C. Zhou, *Chem. Soc. Rev.* **2012**, *41*, 7761–7779.
[5] "Issues Affecting Adoption of Natural Gas in Light- and Heavy-Duty Vehicles": G. A. Whyatt, **2010**, PNNL-19745.
[6] V. C. Menon, S. Komarneni, *J. Porous Mater.* **1998**, *5*, 43–58.
[7] J. Wegrzyn, M. Gurevich, *Appl. Energy* **1996**, *55*, 71–83.
[8] Y. He, W. Zhou, G. Qian, B. Chen, *Chem. Soc. Rev.* **2014**, *43*, 5657–5678.
[9] B. Li, H.-M. Wen, W. Zhou, J. Q. Xu, B. Chen, *Chem* **2016**, *1*, 557–580.
[10] S. M. Cohen, *Chem. Rev.* **2012**, *112*, 970–1000.
[11] U. Stoeck, S. Krause, V. Bon, I. Senkovska, S. Kaskel, *Chem. Commun.* **2012**, *48*, 10841–10843.
[12] M. Zhang, W. Zhou, T. Pham, K. A. Forrest, W. Liu, Y. He, H. Wu, T. Yildirim, B. Chen, B. Space, Y. Pan, M. J. Zaworotko, J. Bai, *Angew. Chem. Int. Ed.* **2017**, *56*, 11426–11430; *Angew. Chem.* **2017**, *129*, 11584–11588.
[13] J. A. Mason, M. Veenstra, J. R. Long, *Chem. Sci.* **2014**, *5*, 32–51.
[14] F. Gándara, H. Furukawa, S. Lee, O. M. Yaghi, *J. Am. Chem. Soc.* **2014**, *136*, 5271–5274.
[15] Y. Yan, D. I. Kolokolov, I. da Silva, A. G. Stepanov, A. J. Blake, A. Dailly, P. Manuel, C. C. Tang, S. Yang, M. Schroder, *J. Am. Chem. Soc.* **2017**, *139*, 13349–13360.
[16] Y. Peng, V. Krungleviciute, I. Eryazici, J. T. Hupp, O. K. Farha, T. Yildirim, *J. Am. Chem. Soc.* **2013**, *135*, 11887–11894.
[17] C. E. Wilmer, M. Leaf, C. Y. Lee, O. K. Farha, B. G. Hauser, J. T. Hupp, R. Q. Snurr, *Nat. Chem.* **2012**, *4*, 83–89.
[18] Y. G. Chung, J. Camp, M. Haranczyk, B. J. Sikora, W. Bury, V. Krungleviciute, T. Yildirim, O. K. Farha, D. S. Sholl, R. Q. Snurr, *Chem. Mater.* **2014**, *26*, 6185–6192.
[19] C. M. Simon, J. Kim, D. A. Gomez-Gualdron, J. S. Camp, Y. G. Chung, R. L. Martin, R. Mercado, M. W. Deem, D. Gunter, M. Haranczyk, D. S. Sholl, R. Q. Snurr, B. Smit, *Energy Environ. Sci.* **2015**, *8*, 1190–1199.

[20] M. Fernandez, T. K. Woo, C. E. Wilmer, R. Q. Snurr, *J. Phys. Chem. C* **2013**, *117*, 7681–7689.
[21] Y. Bao, R. L. Martin, C. M. Simon, M. Haranczyk, B. Smit, M. W. Deem, *J. Phys. Chem. C* **2015**, *119*, 186–195.
[22] Y. Bao, R. L. Martin, M. Haranczyk, M. W. Deem, *Phys. Chem. Chem. Phys.* **2015**, *17*, 11962–11973.
[23] Y. J. Colón, D. A. Gómez-Gualdrón, R. Q. Snurr, *Cryst. Growth Des.* **2017**, *17*, 5801–5810.
[24] D. A. Gomez-Gualdron, O. V. Gutov, V. Krungleviciute, B. Borah, J. E. Mondloch, J. T. Hupp, T. Yildirim, O. K. Farha, R. Q. Snurr, *Chem. Mater.* **2014**, *26*, 5632–5639.
[25] S. Lee, B. Kim, H. Cho, H. Lee, S. Y. Lee, E. S. Cho, J. Kim, *ACS Appl. Mater. Interfaces* **2021**, *13*, 23647–23654.
[26] D. A. Gómez-Gualdrón, C. E. Wilmer, O. K. Farha, J. T. Hupp, R. Q. Snurr, *J. Phys. Chem. C* **2014**, *118*, 6941–6951.
[27] Z. Chen, M. R. Mian, S.-J. Lee, H. Chen, X. Zhang, K. O. Kirlikovali, S. Shulda, P. Melix, A. S. Rosen, P. A. Parilla, T. Genett, R. Q. Snurr, T. Islamoglu, T. Yildirim, O. K. Farha, *J. Am. Chem. Soc.* **2021**, *143*, 18838–18843.
[28] H. S. Koh, M. K. Rana, A. G. Wong-Foy, D. J. Siegel, *J. Phys. Chem. C* **2015**, *119*, 13451–13458.
[29] C. R. Cioce, Computational Investigations of Potential Energy Function Development for Metal-Organic Framework Simulations, Metal Carbenes, and Chemical Warfare Agents, University of South Florida, **2015**.
[30] C. R. Cioce, K. McLaughlin, J. L. Belof, B. Space, *J. Chem. Theory Comput.* **2013**, *9*, 5550–5557.
[31] Y. G. Chung, E. Haldoupis, B. J. Bucior, M. Haranczyk, S. Lee, H. Zhang, K. D. Vogiatzis, M. Milisavljevic, S. Ling, J. S. Camp, B. Slater, J. I. Siepmann, D. S. Sholl, R. Q. Snurr, *J. Chem. Eng. Data* **2019**, *64*, 5985–5998.
[32] M. G. Martin, J. I. Siepmann, *J. Phys. Chem. B* **1998**, *102*, 2569–2577.
[33] S. L. Mayo, B. D. Olafson, W. A. Goddard, *J. Phys. Chem.* **1990**, *94*, 8897–8909.
[34] A. K. Rappe, C. J. Casewit, K. S. Colwell, W. A. Goddard, W. M. Skiff, *J. Am. Chem. Soc.* **1992**, *114*, 10024–10035.
[35] J. Jiang, H. Furukawa, Y.-B. Zhang, O. M. Yaghi, *J. Am. Chem. Soc.* **2016**, *138*, 10244–10251.
[36] J. K. Schnobrich, O. Lebel, K. A. Cychosz, A. Dailly, A. G. Wong-Foy, A. J. Matzger, *J. Am. Chem. Soc.* **2010**, *132*, 13941–13948.
[37] N. Klein, I. Senkovska, I. A. Baburin, R. Gruenker, U. Stoeck, M. Schlichtenmayer, B. Streppel, U. Mueller, S. Leoni, M. Hirscher, S. Kaskel, *Chem. Eur. J.* **2011**, *17*, 13007–13016.
[38] B. Li, H.-M. Wen, H. Wang, H. Wu, M. Tyagi, T. Yildirim, W. Zhou, B. Chen, *J. Am. Chem. Soc.* **2014**, *136*, 6207–6210.
[39] A. Ahmed, S. Seth, J. Purewal, A. G. Wong-Foy, M. Veenstra, A. J. Matzger, D. J. Siegel, *Nat. Commun.* **2019**, *10*, 1568.
[40] R. A. Dodson, A. G. Wong-Foy, A. J. Matzger, *Chem. Mater.* **2018**, *30*, 6559–6565.
[41] L. Feng, K.-Y. Wang, G. S. Day, M. R. Ryder, H.-C. Zhou, *Chem. Rev.* **2020**, *120*, 13087–13133.
[42] H. Furukawa, K. E. Cordova, M. O'Keeffe, O. M. Yaghi, *Science* **2013**, *341*, 1230444.
[43] J. Ma, A. P. Kalenak, A. G. Wong-Foy, A. J. Matzger, *Angew. Chem. Int. Ed.* **2017**, *56*, 14618–14621; *Angew. Chem.* **2017**, *129*, 14810–14813.
[44] H. Wu, J. M. Simmons, Y. Liu, C. M. Brown, X.-S. Wang, S. Ma, V. K. Peterson, P. D. Southon, C. J. Kepert, H.-C. Zhou, T. Yildirim, W. Zhou, *Chem. Eur. J.* **2010**, *16*, 5205–5214.
[45] S. Ma, D. Sun, J. M. Simmons, C. D. Collier, D. Yuan, H.-C. Zhou, *J. Am. Chem. Soc.* **2008**, *130*, 1012–1016.
[46] H. Wu, W. Zhou, T. Yildirim, *J. Am. Chem. Soc.* **2009**, *131*, 4995–5000.

[47] J. I. Feldblyum, D. Dutta, A. G. Wong-Foy, A. Dailly, J. Imirzian, D. W. Gidley, A. J. Matzger, *Langmuir* **2013**, *29*, 8146–8153.

[48] L. D. Tran, J. I. Feldblyum, A. G. Wong-Foy, A. J. Matzger, *Langmuir* **2015**, *31*, 2211–2217.

[49] M. Eddaoudi, J. Kim, N. Rosi, D. Vodak, J. Wachter, M. O'Keeffe, O. M. Yaghi, *Science* **2002**, *295*, 469–472.

[50] H. Furukawa, N. Ko, Y. B. Go, N. Aratani, S. B. Choi, E. Choi, A. Ö. Yazaydin, R. Q. Snurr, M. O'Keeffe, J. Kim, O. M. Yaghi, *Science* **2010**, *329*, 424–428.

[51] D. Alezi, Y. Belmabkhout, M. Suyetin, P. M. Bhatt, L. J. Weselinski, V. Solovyeva, K. Adil, I. Spanopoulos, P. N. Trikalitis, A.-H. Emwas, M. Eddaoudi, *J. Am. Chem. Soc.* **2015**, *137*, 13308–13318.

[52] J. Goldsmith, A. G. Wong-Foy, M. J. Cafarella, D. J. Siegel, *Chem. Mater.* **2013**, *25*, 3373–3382.